All-fiber Mach–Zehnder interferometer with dual-waist PCF structure for highly sensitive refractive index sensing

Peng Gao[1] · Yiping Gao[2] · Meiyue Li[3] · Songwei Liu[1] · Ya-nan Zhang[3]

Abstract

A simple, highly sensitive, and all-fiber Mach–Zehnder interferometer (MZI) refractive index (RI) sensor was proposed and experimentally demonstrated, which was fabricated by welding a dual-waist photonic crystal fiber (DWPCF) with two single-mode fibers. The two waists in the PCF, which acted as splitter and combiner of the MZI, could be simply formed by fusion-tapering technique. The high-order cladding modes could be largely excited in the first waist region and propagated along the cladding until the second waist region, where it would be returned into the fiber core and interfered with the core mode. When the RI around the DWPCF changed, an effective RI variation of the cladding modes might generate, which resulted in the shift of interference spectrum. Therefore, the external RI variation could be obtained by monitoring the wavelength position of the interference pattern. Experimental results showed that the interference wavelength shifted with the increase of the external RI, and high measurement sensitivity of 263.5 nm/RIU was achieved with good linearity.

1 Introduction

As a representative physical parameter, refractive index (RI) measurement has important applications in industrial production, medical testing, biochemical sample analysis, food safety, and other fields [1]. Therefore, it is especially significant to measure the RI of a substance quickly and accurately. In recent years, RI sensor based on optical fiber technology has attracted great attentions, since their advantages of small volume, fast response, flexible structure design resist to electromagnetic interference, anti-corrosion, the potential of remote sensing, and so on [2, 3].

In general, the optical fiber RI sensors can be classified into fiber-grating sensors [4, 5], surface plasmon resonance sensors [6–8], Fabry–Perot sensors [9], and Mach–Zehnder

✉ Ya-nan Zhang
zhangyanan@ise.neu.edu.cn

1 Shenyang Normal University, Shenyang 110819, China

2 Liaoning Institute of Standardization, Shenyang 110003, China

3 College of Information Science and Engineering, Northeastern University, Shenyang 110819, China

interferometer (MZI) sensors based on thin core fiber [10], photonic crystal fiber (PCF) [11], few mode fiber [12], and tapered fiber [13, 14], and so on. Among them, the PCF-based MZI sensors are widely used in sensing applications due to its great flexibility in structural design and low-temperature sensitivity [15, 16]. Besides, it is much easier to excite high-order mode in PCF when compared to SMF, which is benefit for realizing high-sensitive RI sensing. In 2014, Zhao et al. demonstrated an MZI RI sensor using a tapered PCF structure, whose sensitivity was 51.902 nm/RIU [17]; in 2015, Tan et al. presented an exploratory demonstration of an optical fiber MZI RI sensor by coating graphene on the PCF surface, and the RI sensitivity of the sensor in the range of 1.33–1.38 and 1.38–1.43 reached 9.4 dB/RIU and 17.5 dB/RIU, respectively [18]; in 2017, Zhao et al. proposed another MZI RI sensor based on PCF with half-taper collapse regions, and the sensitivity was improved to 181.96 nm/RIU [19]. Although these results have demonstrated the possibility of PCF-based MZI for the measurement of RI, there also exist some problems such as low sensitivity, low repeatability, poor stability, and easy to break.

In this paper, we propose an all-fiber MZI RI sensor based on a dual-waist photonic crystal fiber (DWPCF). Through theoretical analysis and experimental demonstration, a highly sensitive RI sensor is verified. Besides, the proposed

sensor behaves good stability, robust structure, and can be prepared by simple fusion splicing method.

2 Structure design and principle analysis

Figure 1 shows the schematic structure of the all-fiber MZI RI sensor. It consists of an ASE broadband source, a dual-waist PCF-sensing head, and a BaySpec demodulation module. The PCF-sensing head (see the inset of Fig. 1) was fabricated by welding a PCF with two single-mode fibers (SMFs) and performing the fusion-tapering process of PCF.

As shown in Fig. 2, a broadband light emitted from the ASE source first entered and transmitted through the core of an SMF, and would partially couple to cladding of the PCF at the melting point of SMF and PCF, while the rest light propagated in the fiber core. Then, at the first waist position, more cladding modes will be excited and interacted with measured medium. These excited cladding modes would finally couple back into the fiber core of the PCF at the second waist position and the second melting point of SMF and PCF, where the modal interferences between the core mode and cladding modes were generated due to that their transmission optical paths were different. After then, this interference signal entered into another SMF and received by the BaySpec spectrum analyzer, from which we can observe the resonant wavelength of the interference spectrum.

In the above process, the principle of double-beam MZI can be used as an example to analyze the interference light intensity and interference wavelength, which can be given as [20]

$$I = I_1 + I_2 + 2\sqrt{I_1 I_2} \cos \varphi, \tag{1}$$

$$\lambda_m = \frac{\Delta n_{\text{eff}} L}{m}, \tag{2}$$

where I_1 and I_2 represent the light intensities of core mode and cladding mode of the PCF, respectively; I is the total output light intensity; φ is the phase difference; λ_m represents the m-order resonance wavelength; L is the interference length, which equals to the distance between the two fusion points; and Δn_{eff} is the effective RI difference between the core mode and cladding mode.

When the RI of the external environment changes, the effective RI of the cladding mode changes, while the RI of the core mode remains unchanged. Therefore, the wavelength shift caused by the external RI variation can be expressed as

$$\Delta \lambda_m = \frac{\Delta n L}{m}, \tag{3}$$

where $\Delta \lambda_m$ is the shift of mth-order interference wavelength and Δn is the change in the RI difference between the core and cladding modes that caused by the change in the RI of the external environment. It can be seen from Eq. (3) that the amount of wavelength drift is affected by variation in RI difference Δn. When the interference length is constant, the shift of the resonance wavelength of the interference fringe changes linearly with the variation of Δn. It should
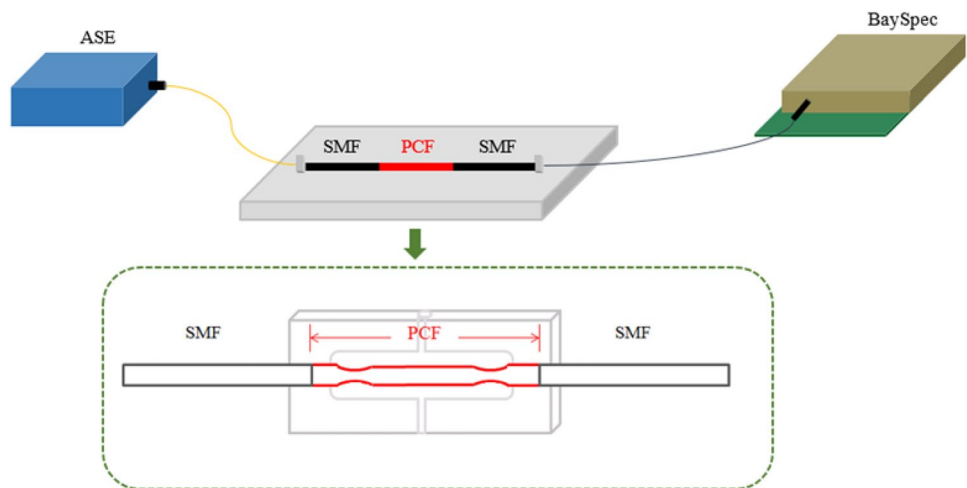
Fig. 1 Schematic structure of sensing system

Fig. 2 Transmission path of light in SMF–TWPCF–SMF-sensing head

be mentioned that there exists more than one cladding mode in the PCF, and any two of them will generate an interference pattern. The final interference spectrum of the proposed sensor is the combination of all double-beam interference spectrum. However, the spectrum shifts on any one of the double-beam interferences will induce the shift of the final interference spectrum. Therefore, the RI of the external medium can be measured by monitoring the shift of the final interference spectrum.

3 Fabrication and building of sensing system

The PCF used in the experiment has five layers of air holes, with fiber diameter of 125.2 μm, air-hole spacing of 7.67 μm, air-hole diameter of 4.88 μm, and core diameter of 8.89 μm. The end face of the PCF is shown in the inset of Fig. 3. During the preparation of the sensor, the SMFs and PCF were welded by a German BAGGER S80A optical fiber fusion splitter using manual mode. The discharge current was 114 mA, the pre-discharge time was 50 ms, and the discharge time was 2 s. The whole length of the PCF was 29 mm. After the left and right ends of the PCF were, respectively, welded to the SMFs, the PCF was tapered by

a fire-breathing device. The structural parameters (diameter and length) of the waist can be controlled by adjusting the pulling speed of the PCF on the fire-breathing device. The images of the two waist regions under an electron microscope are shown in Fig. 3. The left-waist length was 3009.79 μm with a waist diameter of 74.91 μm, while the right-waist length was 4842.69 μm with a waist diameter of 55.47 μm.

During the experiment, the fabricated SMF–TWPCF–SMF-sensing head would be fixed by two magnetic platen fiber clamps on two 3D adjusting platforms and placed in a microfluidic control device, which has a groove and a U-shaped groove extending transversely through the groove. As shown in Fig. 4, the electron microscope was used to observe the structural parameters of the sensing head, and the position of the sensing head could be adjusted using the two 3D adjusting platforms. Then, the fiber was placed in the U-shaped groove (as shown in Fig. 4b), and the TWPCF was in the groove and could be completely immersed in the liquid in the groove. A liquid inlet and a liquid outlet are provided in front of the groove for injecting liquid and discharging liquid. Finally, the sensing head was linked to an ASE-C broadband light source with wavelength range of 1525–1568 nm and a BaySpec's FBGA-F-1525-1605-FA spectral demodulation module.

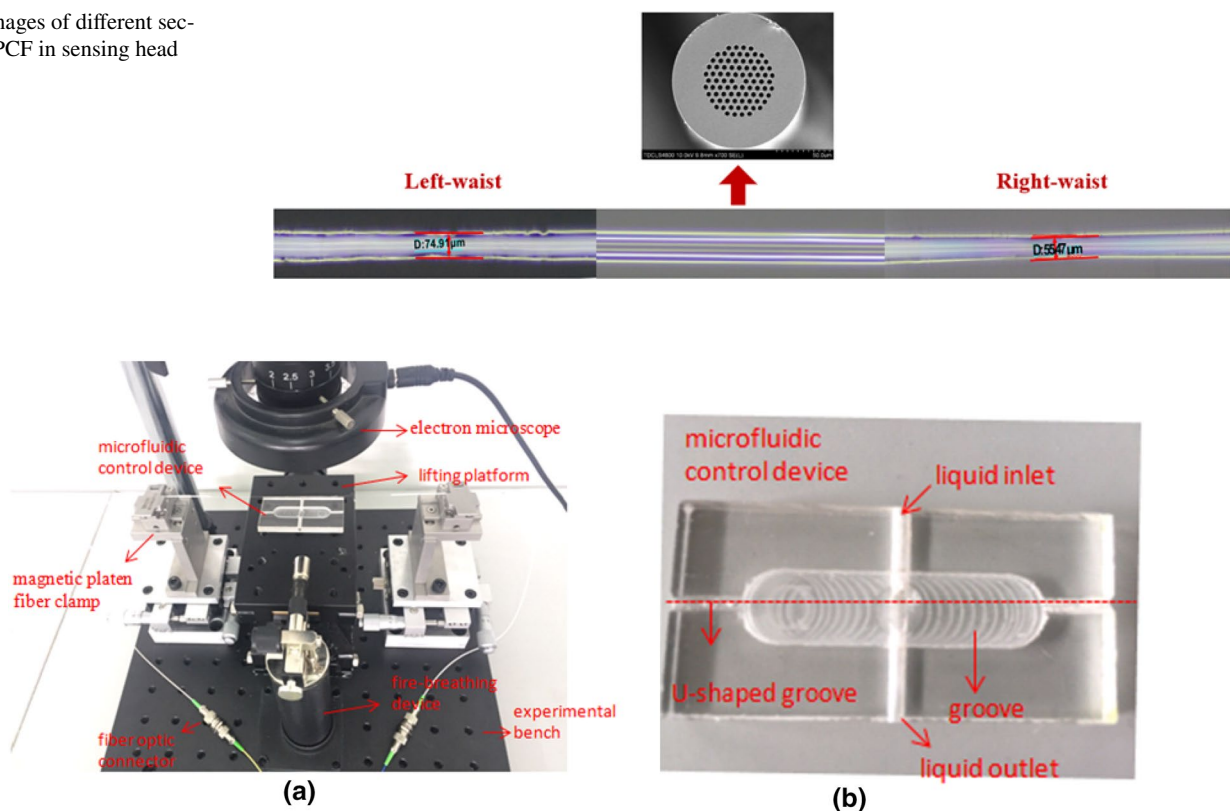**Fig. 3** Images of different sections of PCF in sensing head

Fig. 4 Experimental devices of RI sensor

Table 1 Relationship between concentration of NaCl solution and RI

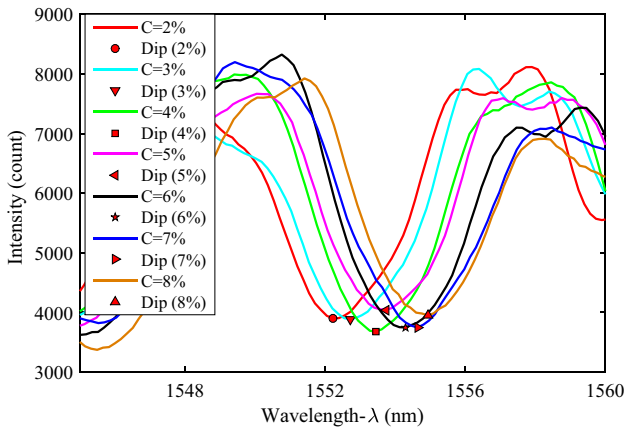| Concentration of NaCl solution C (%)	2	3	4	5	6	7	8
RI (n)	1.3374	1.3388	1.3405	1.3422	1.3441	1.3458	1.3477

Fig. 5 Interference spectrum under different concentrations of NaCl solution
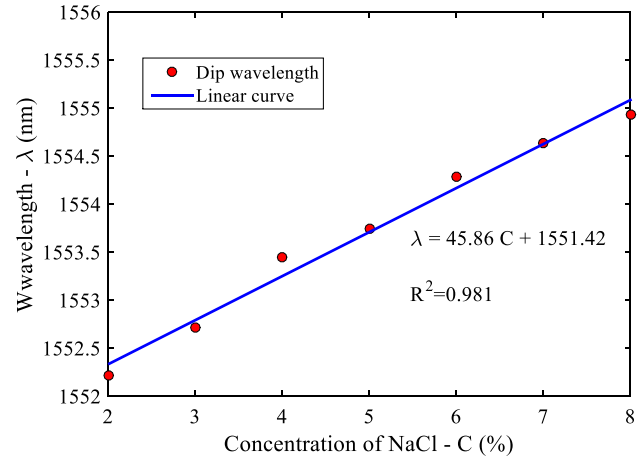

Fig. 6 Relationship between the wavelength of the resonant valley and the concentration of NaCl solution

4 Experiment measurement and discussion

To find the relationship between the wavelength shift of the interference spectrum and the RI change, this paper uses different concentrations of NaCl solution as the test solution, which is cheap, easy to obtain, and easy to precisely adjust the concentration (refractive index). Besides, the Abbe refractometer is used to calibrate the relationship between the NaCl concentration and the RI, as shown in Table 1. The whole experiment was carried out at 24 °C. The prepared NaCl solutions of different concentrations were sequentially injected into the microfluidic control device to observe and record the data of the respective interference spectra. After each set of experiment, the microfluidic control mechanism and the sensing probe should be cleaned by distilled water.

Under different concentrations of NaCl, the interference spectra are shown in Fig. 5. From the data collected by the spectrometer, the relationship between the wavelength value at the resonance valley and the concentration C could be obtained, as shown in Fig. 6. It could be seen that the resonant valley was red shift with the increase of C, whose sensitivity was 0.4586 nm/%, and the linear fit was 0.981. Then, the relationship between the wavelength value at the resonance valley and the RI could also be obtained, as shown in Fig. 7. The RI sensitivity could be 263.5 nm/RIU with high linear fit of 0.971. Compared with the performances of some published optical fiber RI sensors based on MZI [17, 19, 21–24], the measurement
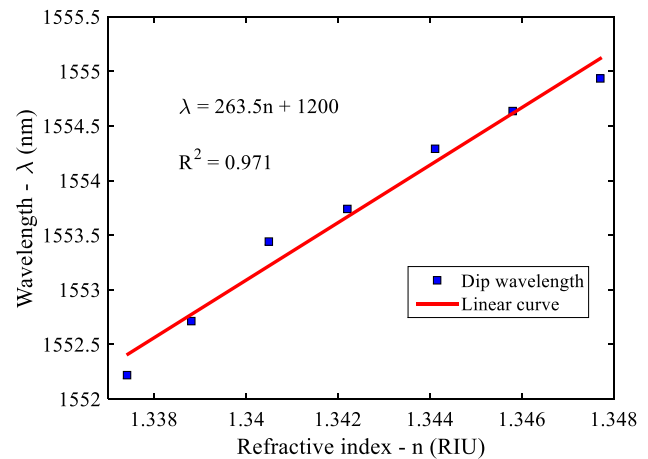

Fig. 7 Relationship between wavelength of resonant valley and RI

sensitivity of this RI sensor is larger than most of the reported results. Besides, the proposed sensor is low cost, simple in fabrication, and robust.

5 Conclusion

A novel MZI RI sensor based on SMF–TWPCF–SMF structure was proposed in this work. The RI measurement experiment was done in a microfluidic control device. Experimental results demonstrated that the resonance valley wavelength shifted with the increase of the RI of the

external NaCl solution. The sensitivity was 263.5 nm/RIU in the range of 1.3374–1.3477, and it had a good linearity. The proposed sensor behaved the advantages of small volume, good stability, high sensitivity, easy preparation, and robust, which were beneficial for practical applications.

References

1. M. Danaie, B. Kiani, Design of a label-free photonic crystal refractive index sensor for biomedical applications. Photon. Nanostruct. Fundam. Appl. **31**, 89–98 (2018)
2. B.Y. Li, Z.C. Sheng, M. Wu et al., Sensitive real-time monitoring of refractive indices and components using a microstructure optical fiber microfluidic sensor. Opt. Lett. **43**(20), 5070–5073 (2018)
3. Y.N. Zhang, T.M. Zhou, B. Han et al., Optical bio-chemical sensors based on whispering gallery mode resonators. Nanoscale **10**, 13832–13856 (2018)
4. Q.Y. Shi, Y.P. Wang, Y.F. Cui et al., Resolution-enhanced fiber grating refractive index sensor based on an optoelectronic oscillator. IEEE Sens. J. **18**(23), 9562–9567 (2018)
5. Y.C. Tan, W.B. Ji, V. Mamidala et al., Carbon-nanotube-deposited long period fiber grating for continuous refractive index sensor applications. Sens. Actuators B Chem. **196**, 260–264 (2014)
6. Z.W. Ding, T.T. Lang, Y. Wang et al., Surface plasmon resonance refractive index sensor based on tapered coreless optical fiber structure. J. Lightw. Technol. **35**(21), 4734–4739 (2017)
7. M.D. Lu, W. Peng, Q. Liu et al., Dual channel multilayer-coated surface plasmon resonance sensor for dual refractive index range measurements. Opt. Express **25**(8), 8563–8570 (2017)
8. S.D. Chu, K. Nakkeeran, A.M. Abobaker et al., Design and analysis of surface-plasmon-resonance-based photonic quasi-crystal fiber biosensor for high-refractive-index liquid analytes. IEEE J. Sel. Top. Quantum Electron. **25**(2), 6900309 (2019)
9. P.C. Chen, X.W. Shu, H.R. Cao, Novel compact and low-cost ultraweak Fabry–Perot interferometer as a highly sensitive refractive index sensor. IEEE Photon. J. **9**(5), 7105810 (2017)
10. T.H. Xia, A.P. Zhang, B.B. Gu et al., Fiber-optic refractive-index sensors based on transmissive and reflective thin-core fiber modal interferometers. Opt. Commun. **283**(10), 2136–2139 (2010)
11. Q. Wang, L.X. Kong, Y.L. Dang et al., High sensitivity refractive index sensor based on splicing points tapered SMF-PCF-SMF structure Mach–Zehnder mode interferometer. Sens. Actuators B-Chem. **225**, 213–220 (2016)
12. Z.R. Tong, Y.M. Zhong, X. Wang et al., Research on simultaneous measurement of refractive index and temperature comprising few mode fiber and spherical structure. Opt. Commun. **421**, 1–6 (2018)
13. J.B. Liu, D.N. Wang, L. Zhang, Slightly tapered optical fiber with dual inner air-cavities for simultaneous refractive index and temperature measurement. J. Lightw. Technol. **34**, 4872–4876 (2016)
14. K.W. Li, N. Zhang, N.M.Y. Zhang et al., Birefringence induced Vernier effect in optical fiber modal interferometers for enhanced sensing. Sens. Actuators B-Chem. **275**, 16–24 (2018)
15. L. Melo, G. Burton, P. Kubik et al., Refractive index sensor based on inline Mach–Zehnder interferometer coated with hafnium oxide by atomic layer deposition. Sens. Actuators B-Chem. **236**, 537–545 (2016)
16. N.L.P. Andrews, R. Ross, D. Munzke et al., In-fiber Mach–Zehnder interferometer for gas refractive index measurements based on a hollow-core photonic crystal fiber. Opt. Express **24**(13), 14086–14099 (2016)
17. Y. Zhao, D. Wu, Q. Wang, All-fiber Mach–Zehnder interferometer using a tapered photonic crystal fiber for refractive index measurement. IEEE Sens. **2014**, 1080–1083 (2014)
18. Y.C. Tan, Z.Q. Tou, K.K. Chow et al., Graphene-deposited photonic crystal fibers for continuous refractive index sensing applications. Opt. Express. **23**(24), 31286–31294 (2015)
19. Y. Zhao, F. Xia, H.F. Hu et al., A novel photonic crystal fiber Mach–Zehnder interferometer for enhancing refractive index measurement sensitivity. Opt. Commun. **402**, 368–374 (2017)
20. C.P. Lin, Y. Wang, Y.J. Huang et al., Liquid modified photonic crystal fiber for simultaneous temperature and strain measurement. Photon. Res. **5**(2), 129–133 (2017)
21. Y. Zhao, X.G. Li, L. Cai et al., Refractive index sensing based on photonic crystal fiber interferometer structure with up-tapered joints. Sens. Actuators B-Chem. **221**, 406–410 (2015)
22. M.Z. Zhang, G.X. Zhu, L.D. Lu et al., Refractive index sensor based on ultrafine tapered single-mode nocladding single-mode fiber structure. Opt. Fiber Technol. **48**, 297–302 (2019)
23. Y. Dong, S.Y. Xiao, B.L. Wu et al., Refractive index and temperature sensor based on d-shaped fiber combined with a fiber Bragg grating. IEEE Sens. J. **19**(4), 1362–1367 (2019)
24. Y.Q. Ma, D. Guo, Y.Y.L. Gao et al., High sensitive Z-shaped fiber interferometric refractive index sensor: simulation and experiment. IEEE Photon. Technol. Lett. **30**(12), 1131–1134 (2018)